Journal of Materials Chemistry

Cite this: J. Mater. Chem., 2011, 21, 14466

www.rsc.org/materials

PAPER

Pillar effect on cyclability enhancement for aqueous lithium ion batteries: a new material of β-vanadium bronze $M_{0.33}V_2O_5$ (M = Ag, Na) nanowires†

Yang Xu,[a] Xiaosan Han,[a] Lei Zheng,[a] Wensheng Yan[b] and Yi Xie*[a]

Received 1st May 2011, Accepted 17th June 2011
DOI: 10.1039/c1jm11910a

Aqueous lithium ion batteries (LIBs) can fundamentally resolve the safety problem arising from the use of highly toxic and flammable organic solvents, and effectively reduce the manufacturing cost. But many reported aqueous lithium ion battery systems have shown poor stability with capacity retention decreasing rapidly. Taking the silver vanadium oxide (SVO) system as an example, this work focuses on the influence of crystal structural stability on the cycle performance of electrode materials in aqueous electrolyte. β-Vanadium bronze $M_{0.33}V_2O_5$ (M = Ag, Na) nanowires were fabricated through a facile precursor-treatment route and, for the first time, used as anode candidates for aqueous lithium ion batteries. The electrochemical measurements showed that $M_{0.33}V_2O_5$ nanowires with 3D tunneled crystal structure exhibited enhanced cycle performance compared with $Ag_2V_4O_{11}$ nanobelts with 2D layered crystal structure. This improvement is attributed to the crystallographic "pillar effect" which can prevent the structural collapse and crystallinity loss during lithium insertion and extraction. Therefore, our investigation could be helpful for the future design of new materials with optimum crystal structure and beneficial matrix elements to realize the suppression of structural destruction and, as a result, the improvement of cyclic stability for aqueous lithium ion batteries.

Introduction

Although non-aqueous lithium ion batteries (LIBs) are considered to be the most successful electrochemical device with a high available energy density, they usually suffer from the increasing criticism of certain drawbacks, such as safety concerns due to the flammability of the organic electrolyte and the reactivity of the electrode materials with the organic electrolytes in the case of improper use such as overcharging or short-circuiting.[1,2] Furthermore, the special cell assembly technology required during manufacturing steps and the costly organic electrolyte with low ion conductivity deeply limit their application on a large scale. As an attractive alternative to circumvent these problems, aqueous lithium ion batteries (aqueous LIBs) have received much attention in recent years.[3–9] This new kind of second lithium ion battery adopts a "rocking-chair" concept similar to non-aqueous lithium ion batteries and uses a weak alkaline or neutral aqueous solution as the electrolyte.[10] With this combination, the safety problem arising from the use of an organic electrolyte is fundamentally resolved, and the rigorous assembly conditions can also be avoided. Additionally, aqueous LIBs do not need to use strong acidic or alkaline electrolyte and thereby appear to be a more environmental friendly and safer device, which makes them the promising "green" batteries.

In the search for proper Li^+ insertion electrodes, vanadium oxides have been widely studied as potential battery materials since they have several intrinsic advantages such as large capacity, high voltage, and excellent kinetics arising from their layered nature.[11] Their major drawback, however, is the tendency for irreversible phase transformation or even amorphization upon repetitive electrochemical lithiation and delithiation, which causes the declining capacity retention and limits their utility.[12] Although many studies have shown that adding a second metal cation into the structure can increase the framework stability upon lithium insertion,[13–15] recent research on LiV_3O_8 has shown that deterioration of the crystal structure still can be observed to a certain extent during cycling in aqueous electrolyte, resulting in rapid capacity fading.[16] In light of this, it is of great importance to continue searching for the optimum crystal structure and beneficial matrix element to realize the suppression of structural destruction and, as a result, the improvement of cyclic stability.

As noted above, the starting crystalline layered vanadium oxides are prone to lose their long-range order and become amorphous due to the random stacking of V–O layers during lithium insertion and extraction, although the layers themselves are usually retained. Accordingly, if an appropriate structural

[a]Departmant of Nanomaterials and Nanochemistry, Hefei National Laboratory for Physical Sciences at the Microscale, University of Science and Technology of China, Hefei, Anhui, 230026, P. R. China. E-mail: yxie@ustc.edu.cn; Fax: (+86)-551-360-6266; Tel: (+86)-551-360-3987
[b]National Synchrotron Radiation Laboratory, University of Science and Technology of China, Hefei, Anhui, 230029, P. R. China

† Electronic supplementary information (ESI) available: characterization of $AgVO_3$ nanowires precursor, $Ag_2V_4O_{11}$ nanobelts, $Na_2V_6O_{16}$ nanowires precursor, and $Na_{0.33}V_2O_5$ nanowires. See DOI: 10.1039/c1jm11910a

element is introduced into the structural framework to connect the adjacent layers together, which may be described as the "pillar effect", the optimized structure should be comparatively rigid against lithium insertion and extraction in aqueous electrolyte. Herein, taking the silver vanadium oxides (SVO) system as an example, we illustrate this "pillar effect" on the structural stability of the electrode materials for improving the cycle performance in aqueous electrolyte. $Ag_2V_4O_{11}$ (ε-SVO) and $Ag_{0.33}V_2O_5$ (β-vanadium bronze), both known as common compounds within the SVO system, adopt a monoclinic symmetry and have similar lattice parameters, especially similar crystal structures. As shown in Fig. 1, there are two inequivalent vanadium sites of V(1) and V(2) existing in the structure of $Ag_2V_4O_{11}$: $V(1)O_6$ octahedra forming zigzag chains, and $V(2)O_6$ octahedra forming two-leg ladders, respectively. Infinite $[V_4O_{12}]_n$ quadruple strings consisting of these two units are built along the *b*-axis and are further linked by corner-shared oxygen atoms to provide continuous $[V_4O_{11}]_n$ layers along the (001) plane, forming a typical two-dimensional (2D) layered structure with Ag^+ intercalating between the layers.[17] The key structural difference between two SVO compounds lies in the existence of the third vanadium site of V(3) in the structure of $Ag_{0.33}V_2O_5$, where it also forms infinite zigzag chains along the *b*-axis, but in five-fold square pyramidal coordination $V(3)O_5$.[18] Such pyramidal zigzag chains act as the "pillar" to connect the $[V_4O_{11}]_n$ layers by corner-shared oxygen atoms, which changes the 2D layered structure into a 3D tunneled structure. Apparently, this change can effectively alleviate structural collapse and crystallinity loss during repetitive electrochemical lithiation and, thereby, play a key role in enhancing the cyclability of the anode materials under the consideration such that both compounds have a similar element composition and electrochemical reaction.

Bearing in mind that, with a high aspect ratio and large surface-to-volume ratio, one-dimensional nanostructures can provide a shorter diffusion distance for both lithium ions and electrons, a higher contact area with the electrolyte, and accommodation of the mechanical stress induced by volume change, we report a facile hydrothermal precursor-treatment route to obtain β-vanadium bronze $M_{0.33}V_2O_5$ (M = Ag, Na) nanowires in this work. Their electrochemical properties as anode materials for aqueous lithium ion batteries were investigated and the results showed that, as expected, $M_{0.33}V_2O_5$ nanowires exhibited a notably higher discharge capacity, and more importantly, a much better capacity retention at different current densities compared with $Ag_2V_4O_{11}$ nanobelts. To the best of our knowledge, this is the first investigation on β-vanadium bronze as an electrode material for aqueous LIBs, and our work successfully demonstrates the significant role of the crystallographic "pillar effect" on improving the electrode cyclability in aqueous electrolyte. Understanding this point could be helpful to spark the targeted design of new materials for Li storage application in aqueous LIBs.

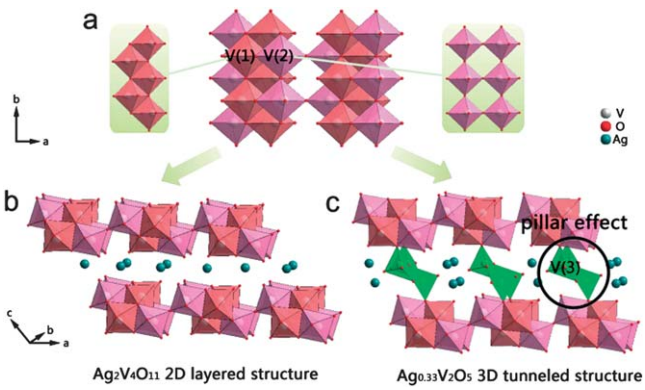

Fig. 1 Illustration of the "pillar effect" for $V(3)O_5$ pyramidal zigzag chains: (a) $[V_4O_{11}]_n$ layer consisting of $V(1)O_6$ octahedra zigzag chains and $V(2)O_6$ octahedra two-leg ladders, (b) $Ag_2V_4O_{11}$ 2D layered structure, and (c) $Ag_{0.33}V_2O_5$ 3D tunneled structure.

Experimental section

All chemical reagents in this work were purchased from Shanghai Chemical Company. They were of analytical grade and used without further purification.

Synthesis of $AgVO_3$ nanowires precursor

0.5 mmol of NH_4VO_3 was added to 30 ml distilled water and the suspension was heated under magnetic stirring until it dissolved to form a clear solution. 0.5 mmol of $AgNO_3$ was dissolved into 10 ml distilled water, and then added dropwise into the above solution. After stirring for 15 min at room temperature, the final mixture was transferred into a 50 ml Teflon-lined stainless steel autoclave, heated at 180 °C for 18 h, and allowed to cool to room temperature naturally. The resulting precipitate was collected by vacuum filtration, washed with distilled water and absolute ethanol several times, and then dried at 60 °C overnight in a vacuum oven.

Synthesis of $Na_2V_6O_{16}$ nanowires precursor

2.0 mmol of anhydrous Na_2SO_4 and 1.0 mmol of V_2O_5 powders were loaded into a 50 ml Teflon-lined stainless steel autoclave, and then 40 ml distilled water was added into it. The autoclave containing the reactant solution was sealed and heated at 200 °C for 24 h, and allowed to cool to room temperature naturally. The resulting precipitate was collected by vacuum filtration, washed with distilled water and absolute ethanol several times, and then dried at 60 °C overnight in a vacuum oven.

Synthesis of β-vanadium bronze $M_{0.33}V_2O_5$ (M = Ag, Na) nanowires

Details of a typical experiment for the synthesis of $M_{0.33}V_2O_5$ nanowires are as follows: 50 mg of corresponding precursor was added to 40 ml distilled water and ultrasonicated for 10 min to give a suspended solution. Then, the pH value of the suspension was adjusted to 1.5∼2.0 using 1.0 mol L^{-1} HNO_3 solution under stirring. After stirring for another 10 min at room temperature, the final mixture was transferred into a 50 ml Teflon-lined stainless steel autoclave to be kept at 200 °C for 24 h, and allowed to cool to room temperature naturally. The resulting precipitate was collected and washed with distilled water and absolute ethanol to remove ions possibly remaining in the final product, and finally dried at 60 °C overnight in a vacuum oven. For comparison, $Ag_2V_4O_{11}$ nanobelts were synthesized using the similar procedures of preparing $AgVO_3$ nanowires except for

adjusting the pH value of the final mixture to ~2.5 using 1.0 mol L^{-1} HNO_3 solution under stirring.

Sample characterization

X-Ray diffraction (XRD) patterns were performed using a Philips X'Pert Pro super diffractometer with Cu-Kα radiation (λ = 1.54178 Å). X-Ray photoelectron spectroscopy (XPS) measurement was performed on a VGESCALAB MKII X-ray photoelectron spectrometer with an excitation of Mg-Kα = 1253.6 eV. Field emission scanning electron microscopy (FESEM) images were taken on a JEOL JSM-6700F scanning electron microscope. Transmission electron microscopy (TEM) image associated with selected area electron diffraction (SAED) and energy dispersive X-ray spectroscopy (EDX) analysis data were obtained by using a JEOL-2010 transmission electron microscope with an acceleration voltage of 200 kV. The near edge X-ray absorption fine structure (NEXAFS) spectra were measured at the U19 beamline of the National Synchrotron Radiation Laboratory (NSRL).

Electrochemical measurement

The electrochemical measurement was performed at ambient temperature. The cyclic voltammograms (CV) were recorded with an electrochemical station (CHI 660B) using a three-electrode system with a saturated calomel electrode (SCE) and Ni foil as the reference and counter electrodes. The preparation of the anode and cathode ($LiMn_2O_4$) electrodes was conducted in a similar way. Test electrodes were prepared by pressing a powdered mixture of the sample, acetylene black (AB), and poly(vinylidene fluoride) (PVDF) in a weight ratio of 80 : 10 : 10, and then dried at 100 °C for 8 h. The electrolyte was an aqueous solution including 5 M $LiNO_3$ and 0.001 M LiOH. The discharge and charge tests for aqueous lithium ion batteries were carried out using the Land battery system (CT2001A) at a constant current density with a cutoff voltage of 1.5~0.4 V.

Results and discussion

The phase and purity of the as-obtained β-vanadium bronze $Ag_{0.33}V_2O_5$ sample were examined through the combined analysis of X-ray diffraction (XRD), X-ray photoelectron spectroscopy (XPS) and near edge X-ray absorption fine structure (NEXAFS). All diffraction peaks in the XRD pattern (Fig. 2a) can be indexed as monoclinic $Ag_{0.33}V_2O_5$ (a = 15.386 Å, b = 3.615 Å, c = 10.069 Å, and β = 109.72°), which is consistent with the values given by JCPDS card No. 81-1740. No peaks from other phases can be detected, indicating that the pure phase of the sample derived from direct hydrothermal treatment of $AgVO_3$ precursor (see Fig. S1†) can be readily realized through our synthetic method. XPS analysis was used to further investigate the chemical composition and state of the as-obtained sample. The XPS survey spectrum in Fig. 2b reveals that our sample only consists of vanadium, silver and oxygen, further showing its high purity. The binding energies obtained in the XPS analysis were corrected for specimen charging by referencing the C 1s to 284.8 eV. The two strong peaks at Ag region of 367.6 and 373.5 eV (Fig. 2c) are, respectively, assigned to Ag^+ $3d_{5/2}$ and $3d_{3/2}$.[19] The V 2p core level spectrum (Fig. 2d)

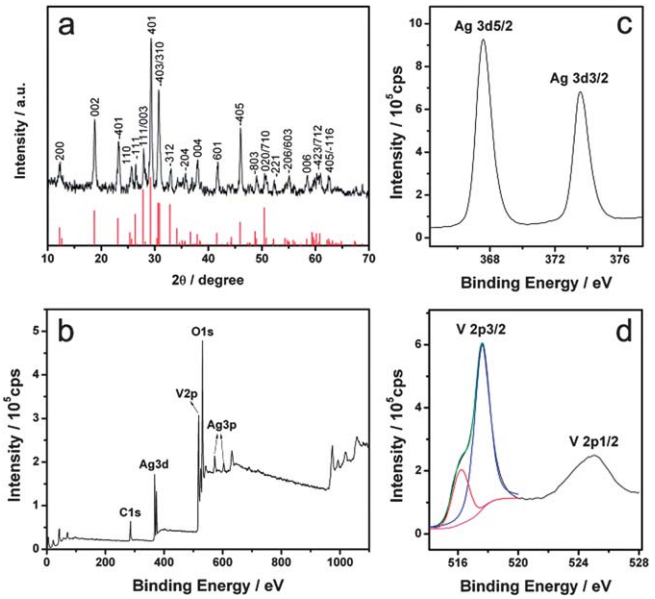

Fig. 2 (a) XRD pattern, (b) XPS survey spectrum, (c) Ag and (d) V high resolution spectra of the as-obtained $Ag_{0.33}V_2O_5$ nanowires.

illustrates two representative peaks centered at 517.6 and 524.8 eV, corresponding to the V $2p_{3/2}$ and V $2p_{1/2}$ of V^{5+}, respectively.[20] The other overlapping peak located at 516.2 eV with less intensity indicates the existence of some amount of V^{4+},[21] confirming the mixture valence state of vanadium atoms in the sample. Such an overlapping phenomenon is usually observed in ternary vanadium bronze compounds containing mixed valences of V^{5+} and V^{4+}.[22–24]

The NEXAFS technique generally measures the resonance features within 50 eV of the absorption edge of the element studied. These resonance features are due to the electronic excitation to partially filled or unfilled molecular orbitals, and as such carry valuable information on the electronic interactions between the bonding elements. Given the selection rules for NEXAFS, $\Delta l = \pm 1$, the V L-edge NEXAFS spectra represent the d electron-projected unoccupied density of states, whereas the O K-edge spectra represent the p electron-projected unoccupied density of states of the valence levels.[25] The NEXAFS data in Fig. 3 show V L-edge and O K-edge regions for the $AgVO_3$ precursor, the as-obtained $Ag_{0.33}V_2O_5$ sample, commercial V_2O_5 and VO_2. The two broad peaks centered around ~516 and ~523 eV can be assigned, in a first approximation, to the V L_3 and L_2 peaks arising from the excitations from V $2p_{3/2}$ and V $2p_{1/2}$ orbitals into empty or partially occupied V 3d states.[26] The spin–orbit splitting between these two peaks is 6.6 eV for V_2O_5, 6.5 eV for $AgVO_3$, 6.4 eV for $Ag_{0.33}V_2O_5$, and 6.2 eV for VO_2. The distinct splitting observed for the β-vanadium bronze sample measured here and in analogy to measurements of bulk samples can be attributed to the presence of a mixed valence of vanadium ions, providing strong evidence for charge disproportionation in its structure. Notably, the low-energy peak located at ~513 eV corresponding to transition into V $3d_{xy}$ levels hybridized with $2p_x/2p_y$ orbitals on the edge-sharing oxygens in V_2O_5 is lost in the β-vanadium bronze sample. This split-off conduction band peak is thought to be responsible for the n-type

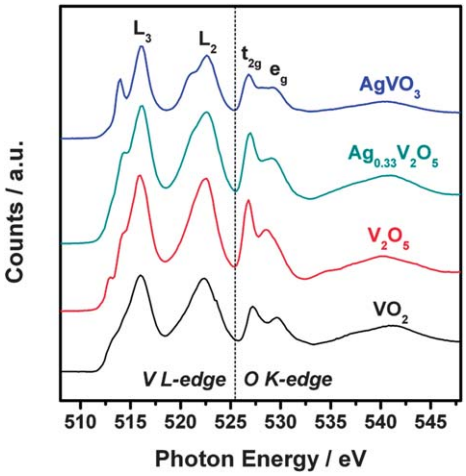

Fig. 3 NEXAFS data for $AgVO_3$ precursor, the as-obtained $Ag_{0.33}V_2O_5$ sample, commercial V_2O_5 and VO_2.

semiconducting nature of V_2O_5 that is no longer retained in β-vanadium bronze sample.[27,28] The V L_2 peak is broadened by the Coster Kronig Auger decay process into a $2p_{3/2}$ hole that does not exist for the L_3 excitation and is less useful for understanding the electronic structure of the nanowires although the splitting of the peaks described above is indeed discernible. In the higher energy region of more than 525 eV, the splitting of the O K-edge spectra into distinct features arises from the crystal field splitting of the V $3d_{z^2}$ and $3d_{x^2-y^2}$ e_g (~529 eV) from V $3d_{xy}$, $3d_{yz}$, and $3d_{xz}$ t_{2g} (~527 eV) levels as a result of the roughly cubic field.[27,28]

The size and morphology of the as-obtained $Ag_{0.33}V_2O_5$ nanowires were examined by field emission scanning electron microscopy (FESEM). The images (Fig. 4a,b) show that the as-obtained sample consists of a large quantity of uniform 1D nanowires with the diameters of 80~100 nm and typical lengths of several tens of micrometres. A good morphological heritage from the precursor was realized under the current hydrothermal treatment (Fig. S1†). It should be noted that the sample has a similar morphology to $Ag_2V_4O_{11}$ nanobelts (Fig. S2†) which will act as a comparison for capacity retention and be discussed later. The TEM image (Fig. 4c) for an individual nanowire further demonstrates that the as-obtained sample has a uniform wire-like morphology. Selected area electron diffraction (SAED) analysis taken from the single nanowire gives a monoclinic ED pattern, revealing its single crystalline nature. The HRTEM image (Fig. 4d) shows the clearly resolved lattice fringes, corresponding to the (−402) and (003) planes. The angle between these planes is 65.5° which is consistent with the SAED pattern. The nanowire shows a preferred [101] orientation. Furthermore, our EDX measurement (Fig. S3†) shows that the sample is composed of Ag, V, and O elements (copper and carbon signals arise from the TEM grid), further indicating its high purity.

β-Vanadium bronze $Ag_{0.33}V_2O_5$, with a high average V valence (4.83), would account for a larger theoretical capacity and better resistance to oxidation by air than other vanadium oxides with low average V valence.[29] A mixed valence of V^{4+}/V^{5+} would give it a higher electronic conductivity and electrochemical reactivity.[29] Due to the crystallographic "pillar effect", the 3D tunneled crystal structure could provide not only an effective pathway for the diffusion of lithium ions but also long-term stability against repetitive lithium insertion and extraction. Herein, for the first time, we investigate the electrochemical properties of $Ag_{0.33}V_2O_5$ nanowires as a new anode material for aqueous LIBs.

The redox behavior related to lithium insertion/extraction of the as-obtained $Ag_{0.33}V_2O_5$ nanowires in aqueous electrolyte was investigated fisrt, and the CV curve is shown in Fig. 5. Two pairs of redox peaks located at 0.077 V/0.074 V and −0.421 V/−0.442 V *versus* a saturated calomel electrode (SCE) can be observed, which are evidently due to a lithium ion intercalation and deintercalation reaction accompanying gain and loss of electrons under the consideration that several geometrically feasible intercalation sites have been identified along the tunneled structure of β-vanadium bronzes[30,31] and occupying the intercalation sites by lithium ions occurs as two-step process in our voltage range.[32] Although the peaks are broad in width, which implies the relatively fast kinetics

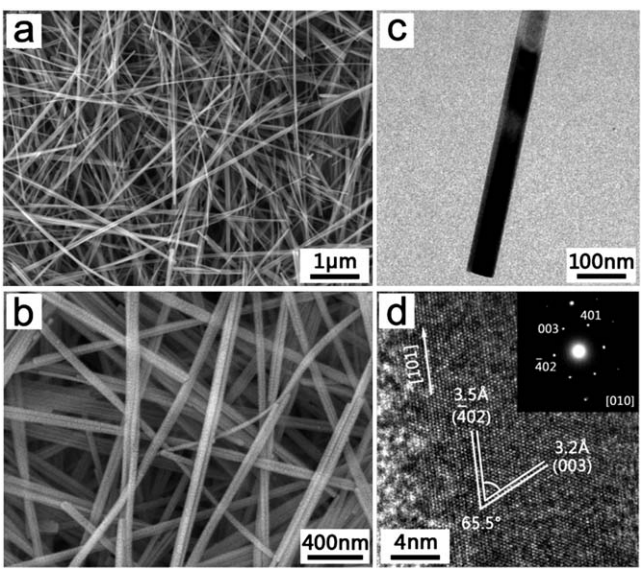

Fig. 4 (a,b) SEM images, (c) TEM image, and (d) HRTEM image and SAED pattern of the as-obtained $Ag_{0.33}V_2O_5$ nanowires.

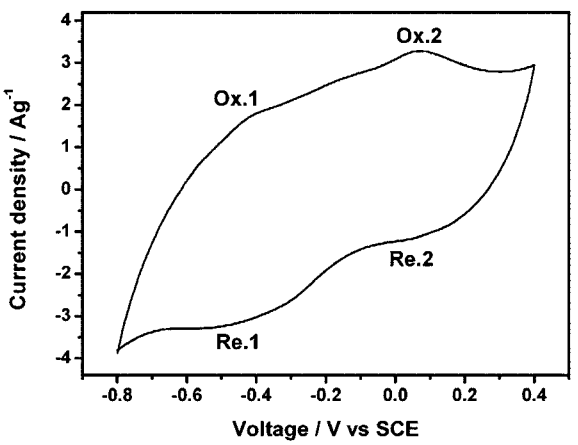

Fig. 5 Cyclic voltammogram of the as-obtained $Ag_{0.33}V_2O_5$ nanowires in aqueous electrolyte at a scan rate of 10 mV s^{-1}. A nickel pellet and SCE were used as the counter electrode and reference electrode. The aqueous electrolyte contains 5 M $LiNO_3$ and 0.001 M LiOH.

of electrode reaction, it is worthy of note that the current density reaches a value as high as 3∼4 A g^{-1} at the scan rate of 10 mV s^{-1}. No obvious H_2 evolution peak is observed, implying that the hydrogen evolution reaction is depressed to a more negative potential. These results indicate that $Ag_{0.33}V_2O_5$ can be used as an anode candidate for aqueous LIBs.

On the basis of CV results, the cell using the as-prepared $Ag_{0.33}V_2O_5$ nanowires as anode was subjected to electrochemical measurement in aqueous solution. Cutoff voltages were set at 0.4 and 1.5 V. The discharge curves of our aqueous cell are shown in Fig. 6a, which summarizes the 1st, 2nd, 50th, and 100th cycle in constant current mode at 60 mA g^{-1}. One can see that the curves have two plateau regions, first around 1.0 V and second in the range of 0.4∼0.6 V. Of note, the cell delivered a first discharge capacity of 103.2 mAh g^{-1}, which is a significant value for aqueous LIB systems in the light of previous reports.[3–5,12,16,33,34] With regard to another important parameter for the cell, the discharge capacity retention and coulombic efficiency (calculated from the ratio of discharge and charge capacity of each cycle) as a function of the cycle number was also investigated, as displayed in Fig. 6b. As can be seen, the reversible discharge capacity after 50 cycles is 73.7 mAh g^{-1}, which is 71.4% of the first discharge capacity. Moreover, this value is still above 50% (54.9 mAh g^{-1}, 53.2%) ever after 100 cycles. For comparison, $Ag_2V_4O_{11}$ nanobelts only keep 27.5% of the first discharge capacity after 30 cycles at the same current density (Fig. S4†), which is much worse than the $Ag_{0.33}V_2O_5$ nanowires. The coulombic efficiency of our cell increased and reached a saturated value after several initial cycles, implying that the electrochemical system had achieved an equilibrium state. The overall average coulombic efficiency is around 97%, further indicating the good reversibility during the long-term charge–discharge tests. Therefore, these results can easily lead to the conclusion that our sample possesses the relatively higher first discharge capacity, and more importantly, a much better capacity retention compared with those of the previously reported aqueous LIBs.[3–5,12,16,33,34]

As expected, the better capacity retention is attributed to the "pillar effect", and to prove this point, electrodes after charge–discharge tests were subject to XRD investigation. As shown in Fig. 7, the diffraction peaks of the sample still exist and no structural change is observed, clearly demonstrating its good structural stability, in spite of the fact that three peaks at 2θ = 38.2, 44.3, and 64.2° belonging to the diffraction of silver emerged arising from the irreversibility of the electrode reaction to a certain extent.[35] With regard to $Ag_2V_4O_{11}$, few crystalline peaks can be observed except for that of silver after 30 cycles compared with its pristine state (Fig. S4†) because of the fact that the 2D layered structure of $Ag_2V_4O_{11}$ collapses due to the significant ionic radii mismatch between silver and lithium ions (r_{Ag^+} = 1.15 Å and r_{Li^+} = 0.76 Å)[36] and the lack of rigidness between V_4O_{11} slabs, resulting in a severe crystallinity loss during the electrochemical process.[35] That is to say, it is because of the "pillar effect" arising from the pyramidal zigzag V(3)O_5 chains which connect the $[V_4O_{11}]_n$ layers and alleviate structural collapse and crystallinity loss that $Ag_{0.33}V_2O_5$ nanowires possess remarkable cyclic stability upon repetitive lithium insertion and extraction, leading to the notable high capacity retention for the aqueous cell.

To further demonstrate the importance of the "pillar effect", we investigated the cyclability of our aqueous cell at different current densities and the retention results are shown in Fig. 8a. As can be seen, the cell still keeps a first discharge capacity of 98.9, 92.9, and 89.1 mAh g^{-1}, respectively, at the current density of 80, 100, and 120 mA g^{-1}. Furthermore, the overall average capacity retention is 64% after 50 cycles and 50% after 100 cycles, respectively. Notably, even when the current density was

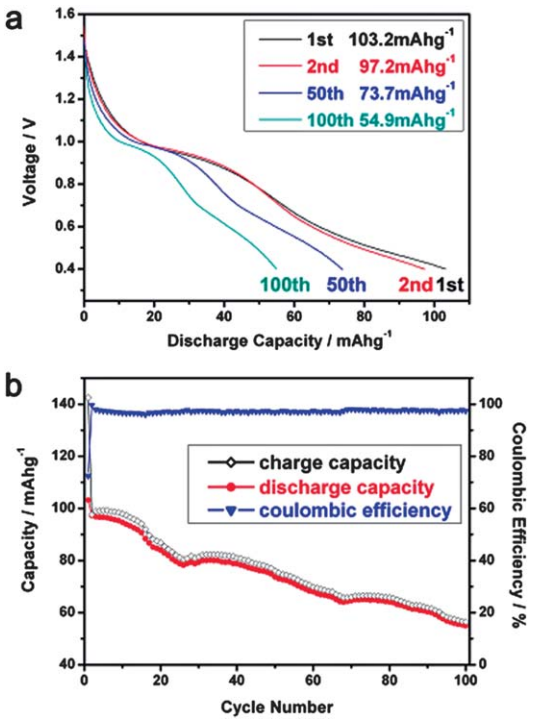

Fig. 6 (a) Voltage *versus* discharge capacity curves of the 1st, 2nd, 50th, and 100th cycle and (b) charge/discharge capacity and coulombic efficiency *versus* cycle number curves of the $LiMn_2O_4/Ag_{0.33}V_2O_5$ cell. The cell was charged and discharged at the current density of 60 mA g^{-1} in aqueous electrolyte.

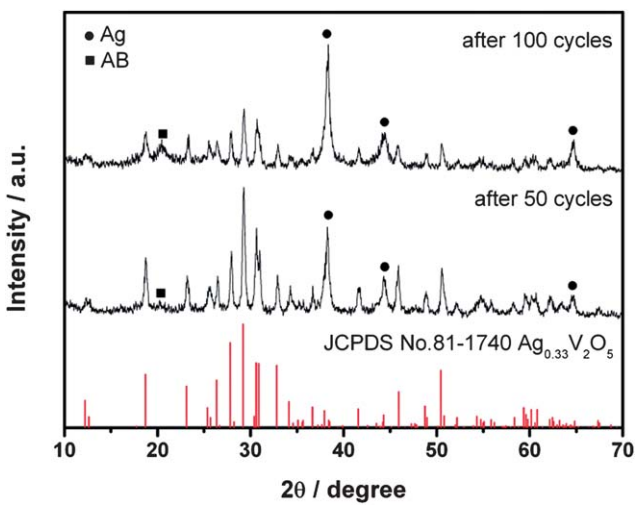

Fig. 7 XRD patterns of $Ag_{0.33}V_2O_5$ nanowires after 50 and 100 charge–discharge cycles at the current density of 60 mA g^{-1}. (AB: acetylene black).

increased by twice as much (120 mA g^{-1}), half of the first discharge capacity still can be delivered after 100 cycles. These results are definitely attributed to the steady crystal structure arising from the "pillar effect", which is validated by XRD examination. As shown in Fig. 8b, we can see that our sample did not show any structural change or degradation after long-term electrochemical process. Crystalline peaks still can be clearly observed and are consistent with the standard pattern (red lines) at different current densities. These results unambiguously give the information that, due to the "pillar effect", the structural stability has been notably improved not only at low current density but also at high current density, which leads to the enhanced capacity retention at different conditions, confirming our cell as a promising candidate for aqueous LIBs.

A further extension should be added that, taking the advantage of this "pillar effect" into account, $Na_{0.33}V_2O_5$ nanowires which were prepared through the similar route of $Ag_{0.33}V_2O_5$ nanowires also exhibited superior cycle performance when used as the anode material for aqueous LIBs. Detailed characterization can be found in the ESI (Fig. S5†) and results of electrochemical investigation are displayed in Fig. 9. The CV curve of the as-obtained $Na_{0.33}V_2O_5$ nanowires in aqueous electrolyte (Fig. 9a) clearly displays two pairs of redox peaks located at 0.267 V/0.100 V and −0.188 V/−0.385 V *versus* SCE, which is evidently due to lithium ion intercalation into and deintercalation from different geometrically feasible sites in the tunneled structure accompanying the gain and loss of electrons.[32] No obvious H_2 evolution peak is observed, implying that the hydrogen evolution reaction is depressed to a more negative potential. The $LiMn_2O_4/Na_{0.33}V_2O_5$ cell has similar discharge curves to the $LiMn_2O_4/Ag_{0.33}V_2O_5$ cell in Fig. 6a, containing two plateau regions (first around 1.2 V and second in the range of 0.4∼0.6 V, Fig. 9b), and even better battery properties than the latter. The electrochemical process delivered a first discharge capacity of 127.5 mAh g^{-1}, which is also a significant value for aqueous LIB systems. Moreover, the reversible discharge capacity is 87.9 and 75.3 mAh g^{-1} after 50 and 100 cycles, respectively, which gives rise to a relatively high capacity retention of 68.9% and 59.1%. In addition, the overall average coulombic efficiency (Fig. 9c) is around 97%, indicating its good reversibility during the long-term charge–discharge tests. Likewise, the nanowires after charge–discharge tests were subject to XRD investigation. The patterns (Fig. 9d) with narrow and intensive peaks did not show any change or degradation after cycles except for the peaks belonging to acetylene black, giving strong further evidence for the important role of the "pillar effect".

Likewise, the $LiMn_2O_4/Na_{0.33}V_2O_5$ cell was cycled at different current densities and the retention results are displayed in Fig. 10a. The first discharge capacity remained almost unchanged with increasing the current density (127.5, 126.6, 125.7, and 123.2 mAh g^{-1} for the current density of 60, 80, 100, and 120 mA g^{-1} respectively). It should be noteworthy that the overall average value of capacity retention is 68.5% after 50 cycles and 51.2% after 100 cycles, also better than $Ag_{0.33}V_2O_5$ nanowires. The XRD patterns of $Na_{0.33}V_2O_5$ nanowires after 100 cycles (Fig. 10b) clearly show that no any change or degradation for the diffraction peaks can be observed at all current densities after such a long-term charge/discharge process, confirming the merit of the "pillar effect" on keeping structural integrity and steady cyclability. Therefore, on the basis of the

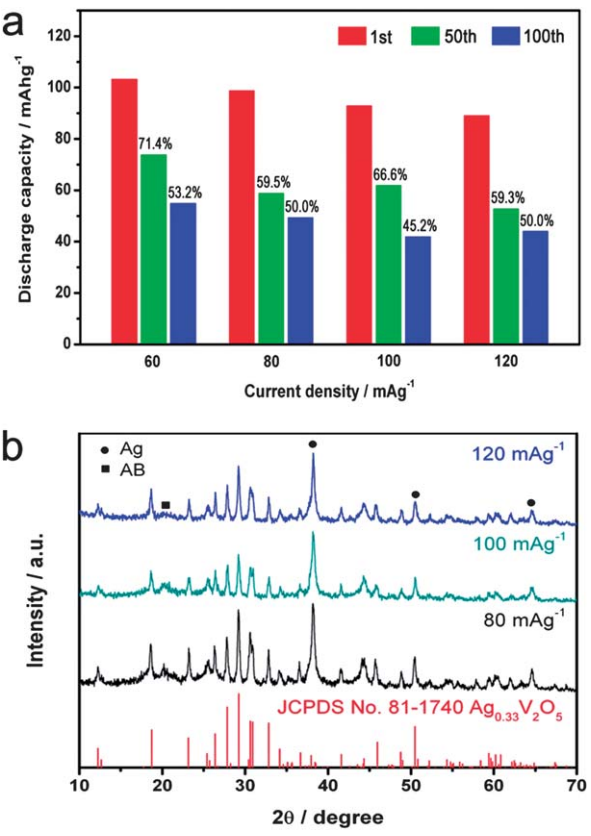

Fig. 8 (a) The discharge capacity of the 1st, 50th, and 100th cycle of the $LiMn_2O_4/Ag_{0.33}V_2O_5$ cell at different current density. (b) XRD patterns of $Ag_{0.33}V_2O_5$ nanowires after 100 cycles at different current density. (AB: acetylene black.)

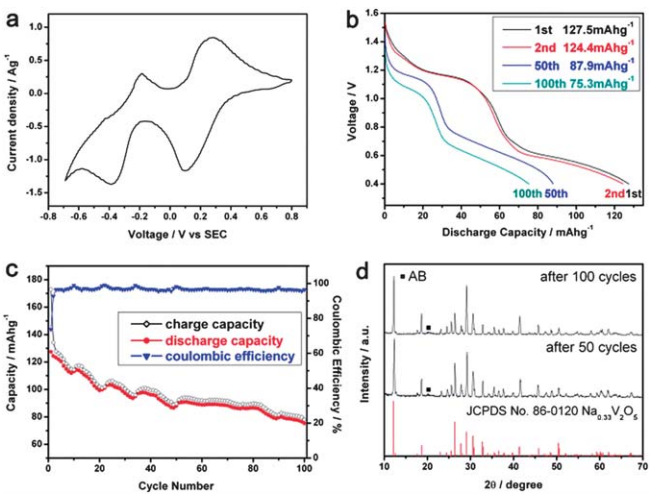

Fig. 9 (a) Cyclic voltammogram of the as-obtained $Na_{0.33}V_2O_5$ nanowires in aqueous electrolyte at a scan rate of 10 mV s^{-1}. (b) Voltage *versus* discharge capacity curves of the 1st, 2nd, 50th, and 100th cycle and (c) charge/discharge capacity and coulombic efficiency *versus* cycle number curves of the $LiMn_2O_4/Na_{0.33}V_2O_5$ nanowires cell. The cell was charged and discharged at the current density of 60 mA g^{-1} in aqueous electrolyte. (d) XRD patterns of the $Na_{0.33}V_2O_5$ nanowires after 50 and 100 charge–discharge cycles. (AB: acetylene black.)

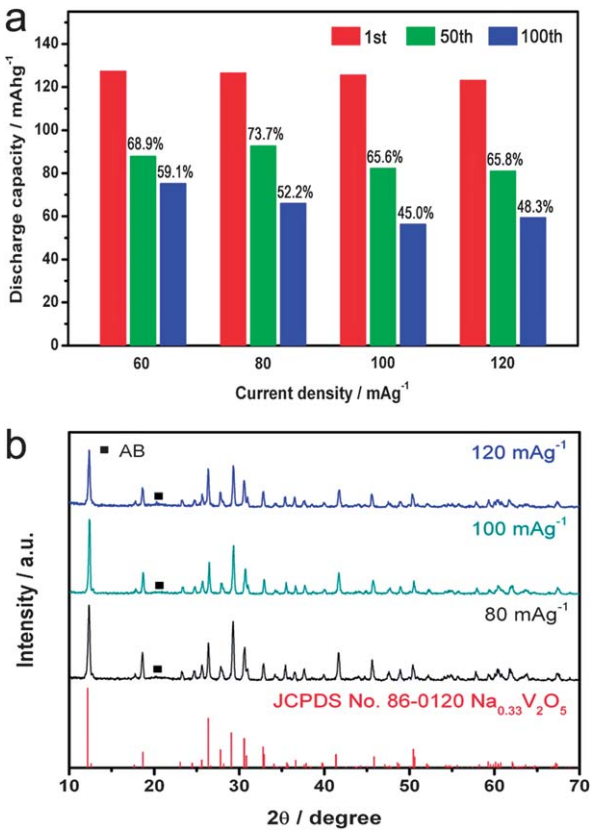

Fig. 10 (a) The discharge capacity of the 1st, 50th, and 100th cycle of the $LiMn_2O_4/Na_{0.33}V_2O_5$ cell at different current densities. (b) XRD patterns of $Na_{0.33}V_2O_5$ nanowires after 100 cycles at different current density. (AB: acetylene black.)

above analysis, $Na_{0.33}V_2O_5$ nanowires give another example to demonstrate that, due to the crystallographic "pillar effect", the 3D tunneled structure exhibits superior stability upon repetitive intercalation/deintercalation of lithium ions, which thereby results in a higher capacity retention for aqueous LIB.

Conclusions

In summary, we have successfully synthesized β-vanadium bronze $M_{0.33}V_2O_5$ (M = Ag, Na) nanowires using a facile precursor-treatment route. The samples are high-quality single-crystalline 1D nanowires with the diameters of ~100 nm and lengths up to several tens of micrometres. As new anode materials for aqueous LIBs, they delivered the relatively high first discharge capacity with over 100 mAh g^{-1}. More importantly, the capacity retention was significantly enhanced compared with $Ag_2V_4O_{11}$ nanobelts and kept a relatively high level at different current densities ranging from ca. 60 to 120 mA g^{-1}. Taking this comparison as an example, our work unambiguously demonstrates that, owing to the crystallographic "pillar effect", the 3D tunneled structure exhibits superior stability than the 2D layered structure upon repetitive lithium intercalation/deintercalation, thereby resulting in higher capacity retention. From the crystallographic point of view, our work provides a valuable way for tackling the challenges of improving the cycle performance of electrode materials in aqueous LIB systems.

Acknowledgements

This work was financially supported by the National Basic Research Program of China (No. 2009CB939901) and National Natural Science Foundation of China (No. 90922016, 10979047, and 11079004).

References

1 M. Armand and J. M. Tarascon, *Nature*, 2008, **451**, 652.
2 J. M. Tarascon and M. Armand, *Nature*, 2001, **414**, 359.
3 G. J. Wang, L. J. Fu, N. H. Zhao, Li. C. Yang, Y. P. Wu and H. Q. Wu, *Angew. Chem.*, 2007, **119**, 299.
4 X. H. Liu, T. Saito, T. Doi, S. Okada and J. Yamaki, *J. Power Sources*, 2009, **189**, 706.
5 S. D. Zhang, Y. M. Li, C. Z. Wu, F. Zheng and Y. Xie, *J. Phys. Chem. C*, 2009, **113**, 15058.
6 C. Z. Wu, Z. P. Hu, W. Wang, M. Zhang, J. L. Yang and Y. Xie, *Chem. Commun.*, 2008, 3891.
7 J. Y. Luo and Y. Y. Xia, *Adv. Funct. Mater.*, 2007, **17**, 3877.
8 Y. Xu, L. Zheng and Y. Xie, *Dalton Trans.*, 2010, **39**, 10729.
9 Y. Xu, L. Zheng, C. Z. Wu, F. Qi and Y. Xie, *Chem.–Eur. J.*, 2011, **17**, 384.
10 W. Li, J. R. Dahn and D. Wainwright, *Science*, 1994, **264**, 1115.
11 M. S. Whittingham, *Chem. Rev. (Washington, DC)*, 2004, **104**, 4271.
12 H. B. Wang, Y. Q. Zeng, K. L. Huang, S. Q. Liu and L. Q. Chen, *Electrochim. Acta*, 2007, **52**, 5102.
13 F. Zhang and M. S. Whittingham, *Electrochem. Commun.*, 2000, **2**, 69.
14 A. Selvaggi, F. Croce and B. Scrosati, *J. Power Sources*, 1990, **32**, 389.
15 F. Garcia-Alvarado and J. M. Tarascon, *Solid State Ionics*, 1994, **73**, 247.
16 J. Kohler, H. Makihara, H. Uegaito, H. Inoue and M. Toki, *Electrochim. Acta*, 2000, **46**, 59.
17 P. Y. Zavalij and M. S. Whittingham, *Acta Crystallogr., Sect. B: Struct. Sci.*, 1999, **55**, 627.
18 C. Sellier, F. Boucher and E. Janod, *Solid State Sci.*, 2003, **5**, 591.
19 J. F. Weaver and G. B. Hoflund, *Chem. Mater.*, 1994, **6**, 1693.
20 G. A. Sawatzky and D. Post, *Phys. Rev. B*, 1979, **20**, 1546.
21 J. Mendialdua, R. Casanova and Y. Barbaux, *J. Electron Spectrosc. Relat. Phenom.*, 1995, **71**, 249.
22 Y. Liu, Y. G. Zhang, M. Zhang and Y. T. Qian, *J. Cryst. Growth*, 2006, **289**, 197.
23 H. Q. Li, T. Y. Zhai, H. Ping, Y. G. Wang, E. Hosono and H. S. Zhou, *J. Mater. Chem.*, 2011, **21**, 1780.
24 J. G. Yu and J. C. Yu, *Mater. Chem. Phys.*, 2007, **104**, 362.
25 D. Ruzmetov, S. D. Senanayake, V. Narayanamurti and S. Ramanathan, *Phys. Rev. B: Condens. Matter Mater. Phys.*, 2008, **77**, 195442.
26 L. Whittaker, C. Jaye, Z. G. Fu, D. A. Fischer and S. Banerjee, *J. Am. Chem. Soc.*, 2009, **131**, 8884.
27 V. Eyert and K. H. Hock, *Phys. Rev. B: Condens.Matter*, 1998, **57**, 12727.
28 E. Goering, O. Muller, M. Klemm, M. L. denBoer and S. Horn, *Philos. Mag. B*, 1997, **75**, 229.
29 C. Tsang and A. Manthiram, *J. Electrochem. Soc.*, 1997, **144**, 520.
30 J. Galy, J. Darriet, A. Casalot and J. B. Goodenough, *J. Solid State Chem.*, 1970, **1**, 339.
31 S. Bach, J. P. Pereira-Ramos, N. Baffier and R. Messina, *J. Electrochem. Soc.*, 1990, **137**, 1042.
32 E. Khoo, J. M. Wang, J. Ma and P. S. Lee, *J. Mater. Chem.*, 2010, **20**, 8368.
33 G. J. Wang, L. J. Fu, B. Wang, N. H. Zhao, Y. P. Wu and R. Holze, *J. Appl. Electrochem.*, 2008, **38**, 579.
34 I. Stojkovic, N. Cujeticanin, I. Pasti, M. Mitric and S. Mentus, *Electrochem. Commun.*, 2009, **11**, 1512.
35 F. Sauvagea, V. Bodenezb, H. Vezinc, M. Morcretteb, J. M. Tarasconb and K. R. Poeppelmeier, *J. Power Sources*, 2010, **195**, 1195.
36 R. D. Shannon, *Acta Crystallogr., Sect. A: Cryst. Phys., Diffr., Theor. Gen. Crystallogr.*, 1976, **32**, 751.

